OXFORD | SOT | Society of Toxicology
academic.oup.com/toxsci

Metabolomics of Lung Microdissections Reveals Region- and Sex-Specific Metabolic Effects of Acute Naphthalene Exposure in Mice

Nathanial C. Stevens [ID],* Patricia C. Edwards,[†] Lisa M. Tran,[‡] Xinxin Ding,[‡] Laura S. Van Winkle [ID],[†] and Oliver Fiehn*,[1]

*UC Davis Genome Center, University of California Davis, Davis, California 95616, USA [†]Center for Health and the Environment, University of California Davis, Davis, California, USA and [‡]Department of Pharmacology and Toxicology, College of Pharmacy, University of Arizona, Tucson, Arizona 85721, USA

[1]To whom correspondence should be addressed at UC Davis Genome Center, University of California Davis, West Coast Metabolomics Center, 451 Health Sciences Drive, Davis, CA 95616, USA. E-mail: ofiehn@ucdavis.edu.

ABSTRACT

Naphthalene is a ubiquitous environmental contaminant produced by combustion of fossil fuels and is a primary constituent of both mainstream and side stream tobacco smoke. Naphthalene elicits region-specific toxicity in airway club cells through cytochrome P450 (P450)-mediated bioactivation, resulting in depletion of glutathione and subsequent cytotoxicity. Although effects of naphthalene in mice have been extensively studied, few experiments have characterized global metabolomic changes in the lung. In individual lung regions, we found metabolomic changes in microdissected mouse lung conducting airways and parenchyma obtained from animals sacrificed at 3 timepoints following naphthalene treatment. Data on 577 unique identified metabolites were acquired by accurate mass spectrometry-based assays focusing on lipidomics and nontargeted metabolomics of hydrophilic compounds. Statistical analyses revealed distinct metabolite profiles between the 2 lung regions. Additionally, the number and magnitude of statistically significant exposure-induced changes in metabolite abundance were different between airways and parenchyma for unsaturated lysophosphatidylcholines, dipeptides, purines, pyrimidines, and amino acids. Importantly, temporal changes were found to be highly distinct for male and female mice with males exhibiting predominant treatment-specific changes only at 2 h postexposure. In females, metabolomic changes persisted until 6 h postnaphthalene treatment, which may explain the previously characterized higher susceptibility of female mice to naphthalene toxicity. In both males and females, treatment-specific changes corresponding to lung remodeling, oxidative stress response, and DNA damage were observed. Overall, this study provides insights into potential mechanisms contributing to naphthalene toxicity and presents a novel approach for lung metabolomic analysis that distinguishes responses of major lung regions.

Key words: metabolomics; lung; microdissection; polycyclic aromatic hydrocarbons.

Naphthalene is a ubiquitous polycyclic aromatic hydrocarbon emitted into the atmosphere by combustion of fossil fuels, cigarette smoke, biomass burning, and several other sources (Jia and Batterman, 2010). Humans are exposed to naphthalene primarily through inhalation but can also ingest naphthalene through diet (Li *et al.*, 2010). Widespread human exposure to naphthalene is of concern due to findings from animal studies that demonstrate acute toxicity as well as formation of neoplasms in rodents, prompting the classification of naphthalene as a potential human carcinogen (NTP, 2000). The proposed mechanism of naphthalene toxicity is through cytochrome P450 (P450) monooxygenase-mediated bioactivation. CYP2F2, the

predominant isoform responsible for metabolizing naphthalene in the mouse lung, rapidly metabolizes naphthalene into a reactive epoxide (Li *et al.*, 2011). This epoxide is detoxified via conjugation with glutathione, but can form DNA and protein adducts upon glutathione depletion, which is accompanied by cytotoxicity in the airway epithelium (Carratt *et al.*, 2019a; Plopper, 2001). The physiological effects of naphthalene exposure include apical membrane blebbing and oxidative stress followed by changes in energy supply and ultimately loss of cells in the airway epithelium (Ling *et al.*, 2014). The human ortholog, CYP2F1, has much lower activity toward naphthalene relative to CYP2F2, which may suggest that humans are at a lower risk for naphthalene-induced tumor formation (Lanza *et al.*, 1999; Shultz *et al.*, 1999). However, transgenic expression of CYP2F1 and CYP2A13, another P450 isoform expressed in human lungs, was sufficient to bioactivate inhaled naphthalene *in vivo* and mediate naphthalene's respiratory toxicity in humanized mice (Li *et al.*, 2017).

Nonciliated lung airway epithelial cells, commonly referred to as club cells, highly express CYP2F2 and are the primary target of naphthalene induced injury in mice (Buckpitt *et al.*, 2002; Phimister *et al.*, 2004; Plopper *et al.*, 1992) regardless of route of exposure. Club cells are most abundant in the distal airways of mice and in the respiratory bronchioles of nonhuman primates and humans (Buckpitt *et al.*, 2002). Airway club cell expression of CYP2F2 in mice is related to site-specific toxicity following naphthalene exposure. Additionally, female mice tend to be more susceptible to the toxic effects of naphthalene, highlighting the importance of both target region- and sex-specific effects of exposure (Carratt *et al.*, 2019b; Van Winkle *et al.*, 2002). Most metabolomics studies use whole organs. However, in the case of naphthalene, the cellular targets of toxicity are club cells which have a restricted distribution in the lung and are confined to the conducting airways. Nonetheless, lung regions that are not targeted for toxicity, and that contain distinct cell types such as the alveolar cell types found in lung parenchyma, may contribute to the initial response. These studies are needed to better understand the mechanisms of naphthalene toxicity that could lead to adverse outcomes in the lung in both target and nontarget regions for acute cytotoxicity.

Metabolomics enables global characterization of metabolites produced by an organism and metabolic changes associated with toxicant exposure or environmental interactions (Bundy *et al.*, 2009; Lankadurai *et al.*, 2013). Previous studies have implemented nontargeted metabolomics analyses to characterize changes in metabolism in response to naphthalene, demonstrating significant alterations with respect to treatment (Lee *et al.*, 2018; Lin *et al.*, 2015). However, these analyses have been limited to the sampling of homogenized whole lung lobes, precluding the ability to distinguish metabolic responses between different lung regions. Identifying these region-specific responses is especially important for toxicants that target-specific cell types with heterogenous distribution throughout the lung (Buckpitt *et al.*, 2013). One potential technique to isolate lung regions is gross lung microdissection, which has previously been established as an approach to distinguish differences in response to naphthalene exposure between lung airways and the surrounding parenchyma (Buckpitt *et al.*, 1995; Plopper *et al.*, 1991).

Our objective was to characterize responses to naphthalene in microdissected lung tissue from male and female mice using nontargeted metabolomics. We treated male and female C57BL/6 mice with a single intraperitoneal injection of naphthalene and sampled gross microdissected airways and parenchyma at 2, 6, and 24 h postinjection. This exposure paradigm has previously demonstrated club cell toxicity similar to acute inhalation of naphthalene in mice (Buckpitt *et al.*, 1995; Kovalchuk *et al.*, 2017; Plopper *et al.*, 1992; Van Winkle *et al.*, 2002). Liquid chromatography—accurate mass tandem mass spectrometry (LC-MS/MS) assays for both lipids and hydrophilic metabolites were implemented to maximize coverage of annotations for both types of tissues. A series of multivariate and univariate statistical analyses were performed to identify metabolite changes among various groups. We hypothesized that metabolite profiles would differ both between tissue types and between treatments. Based on previous studies, we also anticipated female metabolite profiles to be perturbed more than males in response to treatment.

MATERIALS AND METHODS

Animal protocol. Adult male and female C57BL/6 mice (Envigo, Inc.) aged 8–10 weeks were housed on a 12/12 light/dark cycle and fed a diet consisting of Purina 5001 lab diet. Each animal received an i.p. injection of either corn oil, which was used as a vehicle control, or naphthalene dissolved in corn oil (200 mg/kg); all mice were treated at the same time of day, in the morning. Mice were euthanized at 2, 6, or 24 h postinjection with a lethal injection of pentobarbital and necropsied immediately following euthanasia ($N = 6$ per treatment and timepoint for both sexes; $N = 72$ total, 36 male and 36 female). Lungs from each mouse were cannulated, removed *en bloc*, and inflated using a heated solution of 1% agarose (w/v) in 0.01M phosphate-buffered saline. The left lobe of each mouse was microdissected following a previous protocol (Plopper *et al.*, 1991) (Supplementary Figure 1). The resulting airways and parenchyma were immediately stored at -80°C until analysis. All animal experiments were conducted under approved protocols reviewed by the UC Davis Institutional Animal Care and Use Committee in accordance with guidelines for animal research established by the National Institutes of Health.

Preparation of samples and LC-MS/MS analysis. Frozen microdissected tissues were lyophilized for approximately 24 h. Dried samples were homogenized, and 1 mg of dried tissue was used for analysis, roughly equivalent to 10 mg of fresh tissue. Tissue homogenates were extracted on ice in 2-ml centrifuge tubes by adding 225 µl of methanol and an internal standard mixture included in Supplementary Table 1 and 750 µl of methyl *tert*-butyl ether containing cholesterol ester (CE) 22:1 (Cajka and Fiehn, 2016). The top and bottom fractions were evaporated to dryness, which contained hydrophobic and hydrophilic metabolites, respectively. The dry samples containing hydrophilic metabolites were resuspended in 110 µl of 80% acetonitrile, 20% water, and an internal standard mixture included in Supplementary Table 2. The dry samples containing hydrophobic metabolites were resuspended in 100 µl of 90% methanol, 10% toluene, and 50 ng/ml CUDA. Detailed methods for extraction and resuspension can be found in the online data supplement. All samples were analyzed by a ThermoFisher Scientific Vanquish UHPLC+ liquid chromatography system coupled to a Q-Exactive HF orbital ion trap mass spectrometer. Detailed analysis, instrument, and chromatography parameters are included the online Supplementary Data .

Data processing and statistics. Data processing was completed in MS-DIAL v.4.18 (Tsugawa *et al.*, 2015). Identification for all compounds was based on mass spectra from *in silico* libraries, MassBank of North America (https://massbank.us), and NIST20. Experimental spectra from MassBank of North America are publicly available and NIST20 spectra are commercially available

for use. Matches were determined based on *m/z*, retention time, and MS/MS fragmentation pattern (Bonini *et al.*, 2020). The processed data were normalized using systematic error removal in random forest (Fan *et al.*, 2019), a machine-learning algorithm that normalizes experimental samples based on systematic variation in pooled QC samples. Statistical analysis was completed in R v.3.6.1 on the log-transformed dataset. One-way ANOVA was performed with Tukey's HSD *post hoc* test to adjust for multiple comparisons. Multivariate statistical analysis was conducted by principal components analysis (PCA), hierarchical clustering analysis (HCA), and chemical similarity enrichment analysis (ChemRICH) (Barupal and Fiehn, 2017). Volcano plots and heatmaps were generated in R using the Bioconductor packages EnhancedVolcano and ComplexHeatmap (Gu *et al.*, 2016).

RESULTS

Metabolomic and Lipidomics Compound Annotations

A total of 577 unique metabolites were annotated in the dataset across both lipophilic and hydrophilic chromatographic platforms and both electrospray modes (Koelmel *et al.*, 2017). Unknown chromatographic features within the dataset were excluded from the final analysis. The annotations between lipidomics and HILIC analysis were broken down into major classes and is shown in Figure 1. A full list of compounds and classes for all platforms is included online in a Supplementary Data sheet. Among the annotated metabolites analyzed in the study, the values for median relative standard deviation of pooled experimental samples used as a measure of technical variance were 8.3% and 15.5% for compounds identified by lipidomics and HILIC, respectively. Most lipids identified in the dataset were neutral lipids, with a slightly lower number of phospholipids identified. Each major class of lipid was also categorized based on the degree of unsaturation, which can be attributed to biological function. The largest class of hydrophilic metabolites was annotated as derivatives of amino acids included dipeptides.

Metabolic Differences Between Mouse Airways and Parenchyma Dominate Overall Variance

We first determined which experimental factors contributed most to overall differences in the dataset, using PCA as an unbiased multivariate dimension reduction technique (Figure 2). Principal component 1 (PC1) accounted for almost 20% of the overall data variance that was likely due to biological variation between sexes, treatments, and timepoints. Technical errors did not contribute to PC1 variance as seen by the close clustering of the quality control pool samples (Figure 2).
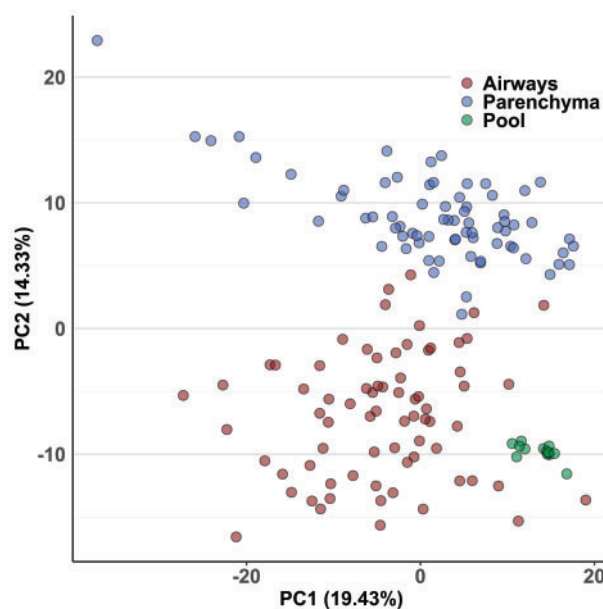

Figure 2. Principal components analysis (PCA) of metabolic variance in mouse lungs. PC2 discriminates metabolic phenotypes of mouse airways and parenchyma. Pool samples were prepared by mixing fractions of each extracted parenchyma and airways sample, which were used as a measure of technical variance of the analytical method.
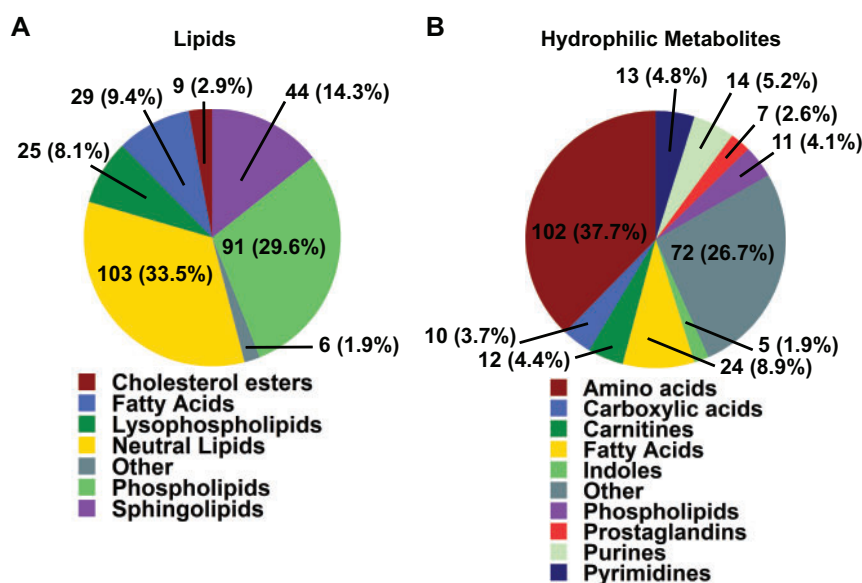

Figure 1. Overview of annotations identified by lipidomics and HILIC analysis. A, Complex lipids were classified by ClassyFire software into 7 major lipid classes consisting of 307 unique annotations. B, Hydrophilic compounds were classified into 10 major metabolite classes, comprising 270 unique annotations. ClassyFire categories with less than 5 compounds were summarized into "Other" class labels.

No single sample needed to be removed due to potential gross difference to all other samples. The next vector, PC2, explained 14.3% of the total data variance, which was attributed to differences in lung airways and parenchyma samples within the dataset. However, differences attributed to sex, naphthalene exposure, or temporal changes did not dominate metabolic phenotypes to an extent that would lead to overt clustering along axes of PCA plots, which typically capture large differences between groups of samples (Supplementary Figure 2) (Ruiz-Perez *et al.*, 2020; Worley and Powers, 2012). Instead, these biological differences led to overall variance with slowly decreasing importance, leading to only 50% explained variance combined by the top 5 principal components (Supplementary Figure 3).

Statistical Analysis of Metabolite Profiles Between Tissues and Naphthalene Treatment

Multivariate analysis identifying changes in metabolite classes between treatments and between tissues was next used to determine differences that contributed to the observed variation by PCA. Chemical enrichment similarity analysis (ChemRICH) enabled characterization of significantly altered metabolite classes in response to naphthalene treatment for both lung airways and parenchyma. ChemRICH is a multivariate statistical approach used as an alternative to traditional pathway mapping that does not rely on database size and groups each metabolite based on its chemical structure, which often alludes to a compound's biological function (Barupal and Fiehn, 2017). Initial ChemRICH analyses between naphthalene-treated and control animals revealed distinct differences at each timepoint and between sexes. In males, amino acids, purines, and several other metabolite classes were altered in response to treatment at 2 h postinjection (Supplementary Figure 4). However, no significant changes in metabolite classes were identified by ChemRICH at 6 or 24 h in males. In contrast, changes in metabolite classes in females were present both at 2 h (Supplementary Figure 5) and at 6 h, with the most extensive changes identified at 6 h postinjection. Dipeptides and unsaturated LPCs were decreased in both airways and parenchyma following naphthalene treatment at 6 h in females, whereas amino acid species were both increased and decreased following treatment (Figs. 3A and 3B). Additionally, multiple pyrimidine nucleosides were decreased in parenchyma but not in airways of the naphthalene-treated animals, highlighting the difference in response between the 2 tissues (Figure 3B). For significantly altered metabolite classes in both airways and parenchyma of females, the average metabolite abundance of each class yielded the greatest fold difference at 6 h comparing the 2 treatment groups (Figs. 3C and 3D). Lastly, ChemRICH analysis comparing metabolite classes between tissues for each sex revealed striking differences in the lipid profiles of airways and parenchyma samples, which were dominated by substantially higher levels of triacylglycerides (TG) in airways than in parenchyma. Importantly, these differences did not appear to be mediated by treatment or sex, as TG abundance was inherently different at each timepoint in the control-treated male and female mice (Supplementary Figure 6).

Following the analysis of metabolite class changes, we next wanted to evaluate alterations within each significantly altered class to identify underlying changes in subclasses of
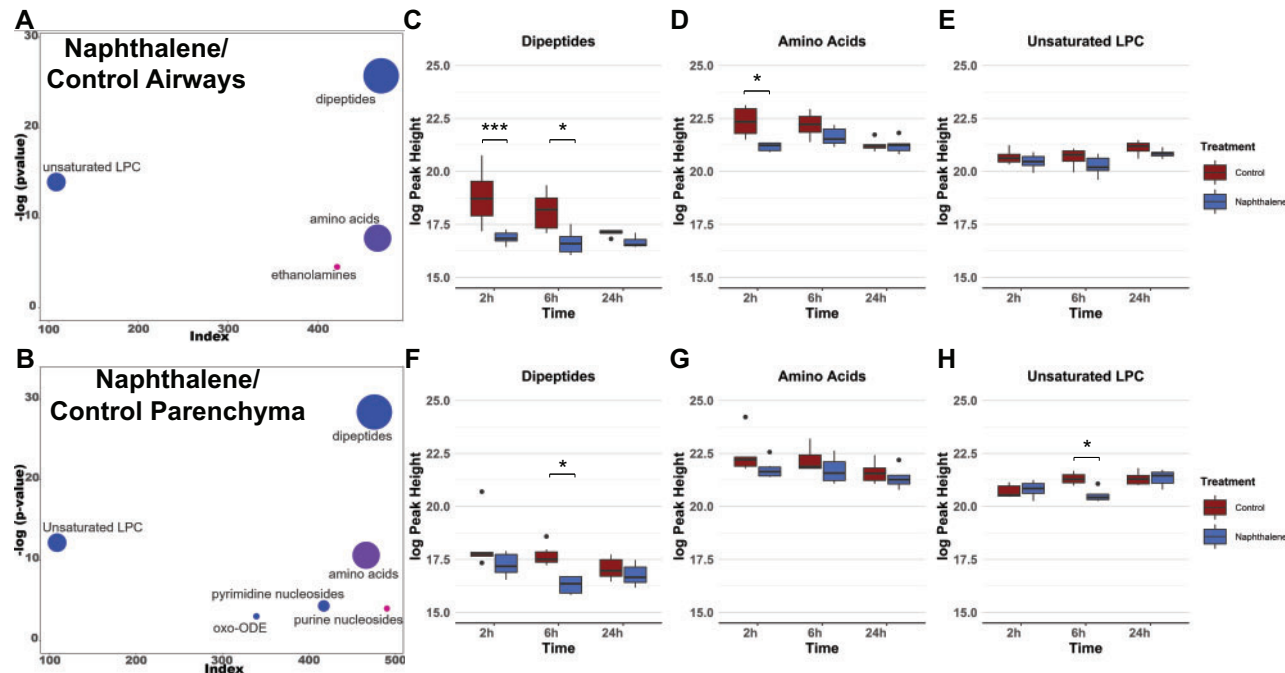

Figure 3. Metabolite profiles of lung airways and parenchyma are altered in response to naphthalene-treatment in females 6 h postinjection. A and B, ChemRICH plots comparing naphthalene-treated airways and parenchyma in female mice 6 h postinjection, respectively. The size of each circle represents the relative number of metabolites contained within each cluster. Red circles indicate all metabolites increase within a cluster, whereas blue circles indicate all metabolites decrease within a cluster. Pink and purple circles represent a mix consisting of mostly increased and decreased metabolite abundances, respectively. Axes correspond to the $-\log p$ value of a metabolite class plotted against index values assigned to each metabolite in the online datasheet included as supplemental material. p values used for the input of each ChemRICH were calculated by 1-way ANOVA with Tukey's *post hoc* analysis. p values for each ChemRICH cluster were calculated using the Kolmogorov-Smirnov test. C–H, Boxplots displaying the average intensities for the largest clusters of metabolite classes altered in female airways and parenchyma for all timepoints, respectively. Axes represent the $\log_{10}$ peak height of each sample for each timepoint, and samples with values greater than 1.5 times the interquartile range are indicated by dots on each plot. $*p < .05$, $***p < .001$.

metabolites related to a specific biological function. Due to the absence of significant differences in metabolite classes in male mice after 2 h, we focused our subsequent analyses on female mice tissues sampled 6 h postinjection. HCA comparing between both tissues and treatments demonstrated several significantly altered metabolites of the same subclass. Once again, unsaturated TGs were more abundant in airways than in parenchyma in the control mice, which were all clustered following HCA. Two clusters, one consisting of unsaturated CE and another consisting of unsaturated phosphatidylcholines (PC) and LPCs were all lower in abundance in airways than in parenchyma in control-treated mice. Interestingly, the fold change in LPCs and PCs decreased in response to naphthalene treatment, whereas the fold change in TGs between both tissues was greatly increased following treatment (Figure 4A).

HCA was also performed for clustering of significant changes comparing the effects of naphthalene treatment on female airways and parenchyma sampled 6 h postinjection (Figure 4B). Purine and pyrimidine derivatives were clustered together and increased in both tissue types following naphthalene treatment, with airways experiencing greater relative increases in several species than parenchyma. Lysine-containing dipeptides and LPCs were also clustered together, which were ubiquitously decreased in response to naphthalene treatment (Figure 4B). The full lists of significantly altered metabolites are included in Supplementary Tables 3 and 4.

Univariate Analysis of Individual Metabolites Significantly Affected by Naphthalene Treatment

Lastly, we analyzed changes in individual metabolite abundance within each tissue type following naphthalene treatment to further distinguish the response of airways compared with parenchyma. For individual metabolite analysis, we also focused on female tissues sampled 6 h postinjection as this timepoint included the greatest number of significantly altered metabolites between sexes and each timepoint. In both airways and parenchyma, adenosine 5′-diphosphoribose (ADP ribose), riboflavin, cytidine 5′-diphosphate ethanolamine, and uridine diphosphate galactose were all altered following naphthalene treatment, passing a threshold $\log_2$ fold change of 5 (Figs. 5A and 5B). However, the fold change of cytidine 5′-diphosphate ethanolamine, ADP ribose, and uridine diphosphate galactose were all relatively greater in airways than in parenchyma, further indicating a tissue-specific response to treatment. Moreover, dipeptides containing lysine residues displayed greater relative fold changes in airways relative to changes in parenchyma. The magnitude of these changes coupled with their biological function may potentially contribute to some of the region-specific effects of naphthalene in mice.

DISCUSSION

Our study demonstrates the importance of region-specific metabolomic analysis of the lung. Previous metabolomics studies of the lung have analyzed homogenized whole lung tissue to characterize the effects of naphthalene in mice (Hong et al., 2014; Lee et al., 2018; Lin et al., 2015; Yao et al., 2016). However, the results of our study demonstrated significant differences when comparing individual regions of microdissected lung tissue from male and female mice that received i.p. injections of naphthalene. PCA displayed clear separation of lung airways and parenchyma regardless of sex, treatment, or time (Figure 2A). Significant variation was present within each tissue, which was most likely attributable to significant differences in
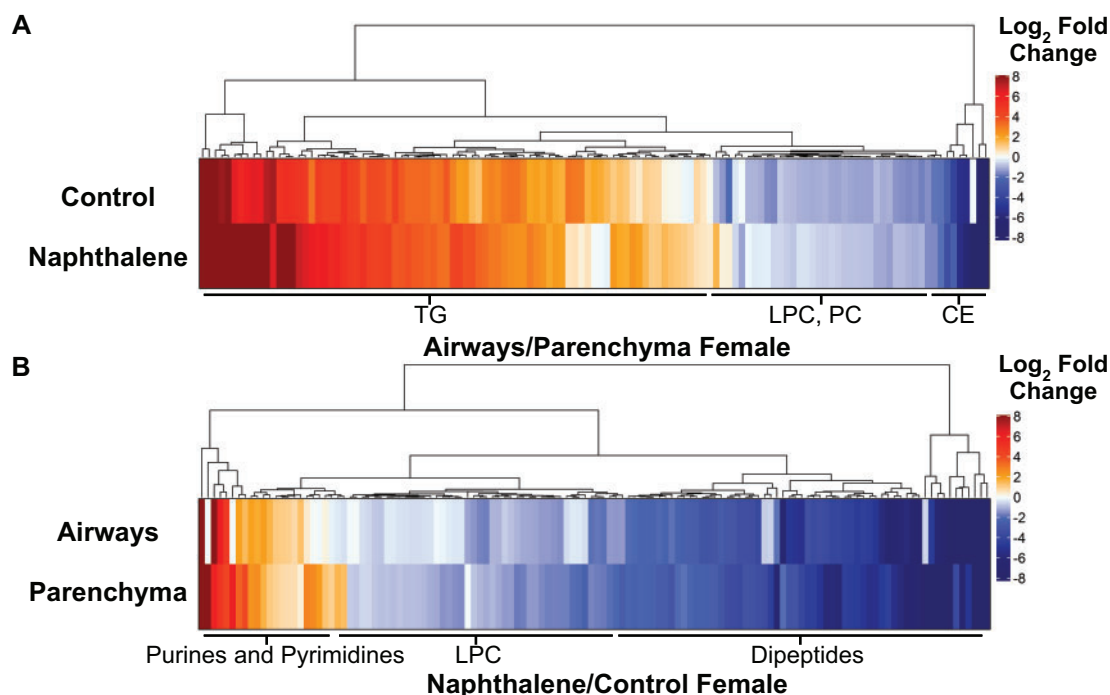

Figure 4. Naphthalene treatment greatly alters the profiles of individual metabolite subclasses in female airways and parenchyma at 6 h. A, Heatmap comparing metabolite abundance of airways relative to parenchyma for each treatment at 6 h. B, Heatmap comparing metabolite abundance of naphthalene-treated tissues relative to control-treated tissues at 6 h for each tissue type. For both heatmaps, Euclidean clustering was used for HCA. Fold changes are expressed as the $\log_2$ fold change of each metabolite to indicate direction. Only metabolites that were statistically significant in at least one comparison were included in each figure. Labels of the most prevalent metabolite classes within each cluster are included below the body of the heatmap. p values were calculated by 1-way ANOVA and Tukey's *post hoc* analysis. Lists of metabolites present in each heatmap are included in Tables 3 and 4.
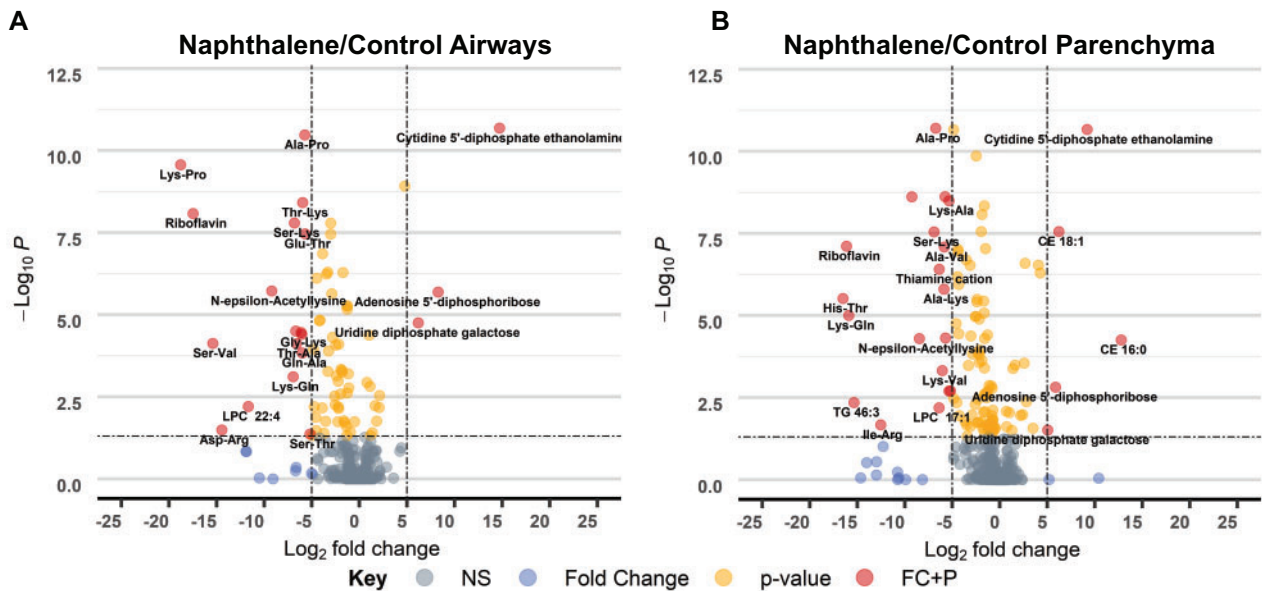
Figure 5. Individual metabolite changes in naphthalene-treated female mice differ in magnitude and between tissues. A and B, Volcano plot of $-\log_{10} p$ value versus $\log_2$ fold change of metabolites in naphthalene-treated airways and parenchyma relative to control, respectively. p values were determined using 1-way ANOVA with Tukey's *post hoc* analysis. An arbitrary $\log_2$ fold change cut-off of 5 was used to indicate metabolites with especially large differences between treatment groups. A p value threshold of $<.05$ was selected to indicate statistical significance. Metabolites that pass both thresholds are indicated in red, whereas metabolites not passing either threshold are shaded in gray. Yellow and blue dots represent metabolites that only pass either the p value or fold change threshold, respectively.

metabolite classes between treatments and timepoints sampled within the study.

ChemRICH analysis and HCA identified metabolite classes and subclass abundances that were unique based on tissue (Figs. 3 and 4). Unsaturated TGs, PCs, and CEs were the predominant metabolite classes that varied in abundance between lung airways and parenchyma, with the relative abundance of unsaturated TGs being much greater in airways compared with PCs and CEs that were less abundant in airways. The relative abundance of these classes following naphthalene treatment shifted significantly, as unsaturated TGs greatly increased in abundance and differences between PCs and CEs became less marked in females at 6 h (Figure 4A). These changes may reflect remodeling of the epithelial cell membrane and lipolysis following cytotoxicity and damage to the epithelium resulting from naphthalene treatment (Lass *et al.*, 2011; Plopper, 2001). Furthermore, intake and export of TGs is dependent upon activity of apolipoprotein E (Apo-E) and apolipoprotein A-I (Apo-AI), respectively. Both proteins are expressed in the lung and serve important roles in maintaining normal lipid metabolism (Yao *et al.*, 2016). Alterations in either Apo-E or Apo-AI are associated with several lung diseases and contribute to increased lung inflammation, oxidative stress, and collagen deposition (Jie Yan *et al.*, 2006; Kim *et al.*, 2010; Rice *et al.*, 2015). Although these studies have not examined the effect of naphthalene treatment on Apo-E and Apo-AI expression, selective TG accumulation in the airways of naphthalene-treated mice may suggest dysregulation of one of these proteins.

Metabolite classes and subclasses were also significantly altered when comparing the effects of naphthalene treatment in females at 6 h postinjection. LPCs and dipeptides were the predominant classes affected by treatment, with dipeptides containing lysine residues constituting several significant differences reported in dipeptide abundance (Figure 4B). LPCs are bioactive lipids formed from phospholipase A$_2$, which can modulate inflammatory responses and are implicated in lung disease (Wang and Tontonoz, 2019; Yoder *et al.*, 2014). LPCs can undergo conversion to PCs through lysophosphatidylcholine acyltransferase (LPCAT)

or can be modified by another enzyme, autotaxin, to lysophosphatidic acid (LPA) (Law *et al.*, 2019). Previous studies have established a potential role of LPA in the development of pulmonary fibrosis through pharmacologic inhibition of the LPA receptor 1, which reduced disease severity in a bleomycin mouse model of pulmonary fibrosis (Ninou *et al.*, 2018; Oikonomou *et al.*, 2012). Significant reductions in LPC following naphthalene treatment may result from increased LPA production or could result from increased production of PCs from LPCs through the Lands' Cycle (Figure 6A) (Wang and Tontonoz, 2019). Concurrent decreases in many glycine, lysine, and proline-containing dipeptides may further support lung remodeling in response to naphthalene treatment considering the role of lysine and proline as important constituents of the extracellular matrix within the lung (Bradley *et al.*, 1974).

Comparisons of individual metabolites were drawn to provide insights into metabolites with unique biological functions in addition to metabolite class changes. Univariate analysis displayed striking alterations in many amino acids and pyrimidine derivatives in both female naphthalene-treated airways and parenchyma at 6 h (Figs. 5A and 5B). Among the metabolites most substantially altered were uridine diphosphate galactose, cytidine 5'-diphosphate ethanolamine, and ADP ribose. Interestingly, the magnitude of fold changes for each of these metabolites was much greater in airways relative to the fold change between naphthalene and control-treated parenchyma. Cytidine 5'-diphosphate ethanolamine is an important precursor used in the synthesis of phosphatidylethanolamines, which are essential components of the cell membrane (Brunetti *et al.*, 1979). The significant increase of this compound in naphthalene-treated mice recapitulates the observed changes in other metabolites following treatment, further implicating remodeling of the cell membrane as an effect of treatment.

Changes in cell membrane characteristics and remodeling may be exacerbated by the effects of significantly reduced lysine and significantly increased ADP ribose also observed following treatment. Lysine has previously been reported to
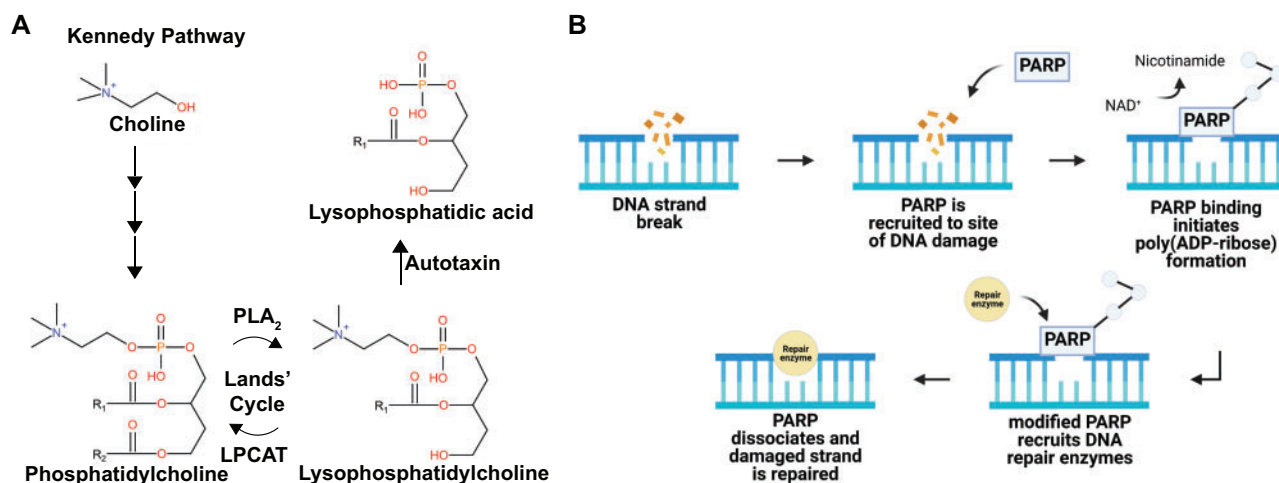
Figure 6. Naphthalene alters metabolites related to lung remodeling, oxidative stress, and DNA damage. A, *De novo* synthesis of phosphatidylcholine (PC) via the Kennedy pathway and subsequent breakdown into lysophosphatidylcholine by phospholipase A_2 (PLA$_2$). Lysophosphatidylcholine can either be metabolized by autotaxin into lysophosphatidic acid or converted back into PC through lysophosphatidylcholine acyltransferase (LPCAT). B, ADP-ribose is a subunit of poly (ADP-ribose), which is formed by poly adenosine diphosphate ribose polymerase (PARP) in response to DNA strand breaks. Created with Biorender.com.

reduce the severity of lipopolysaccharide-induced acute lung injury by reducing lipid peroxidation and proinflammatory responses in mice (Zhang et al., 2019). Reduced abundance of lysine resulting from naphthalene treatment may contribute to increased oxidative stress and glutathione depletion observed in previous studies (Phimister et al., 2004). In addition to glutathione depletion, naphthalene metabolites can form DNA adducts that lead to further cytotoxicity (Carratt et al., 2019a). The substantially increased abundance of ADP ribose, which is a subunit of poly(ADP-ribose) upon DNA damage by poly adenosine diphosphate ribose polymerase (PARP), provides additional evidence supporting these previous findings (Figure 6B) (Altmeyer et al., 2009; Hou et al., 2019; Satoh and Lindahl, 1992). Importantly, the magnitude of this increase was greatest in the airways where ADP ribose abundance was barely detectable in vehicle-treated and several hundred-fold higher in naphthalene-treated female mice at 6 h.

Significant metabolite changes within each tissue following naphthalene treatment were almost exclusively confined to earlier timepoints, with few significant differences remaining between treatment groups 24 h postinjection. This observation may allude to compensatory mechanisms present soon after naphthalene treatment when cells undergo vacuolization and become permeable, which contrasts with the 24-h timepoint where club cells have exfoliated from the epithelial membrane and many are no longer present (Van Winkle et al., 2002). Strikingly, significant metabolic changes were not limited to the airways of naphthalene-treated mice, with similar alterations being present in both airways and parenchyma (Figure 3). Club cells are the primary target for naphthalene toxicity in the mouse lung due to relatively high expression of CYP450 isoforms catalyzing the formation of reactive naphthalene metabolites (Buckpitt et al., 2002). However, cell-to-cell communication is essential for maintaining homeostasis in the lung in response to injury and could potentially affect metabolic responses of other cell types such as those found in the lung parenchyma (Gupta et al., 2019).

When comparing metabolite changes between each sex, male mice displayed significant alterations in multiple metabolite classes at 2 h postinjection (Supplementary Figure 4). In both males and females, the number of significantly altered metabolites was much lower 24 h postinjection (data not shown). However, sex-specific differences in metabolism were most evident when comparing the effect of treatment in lung airways and parenchyma across timepoints. Changes in pyrimidine nucleotide sugars, LPCs, and dipeptides were limited to the 2 h postinjection in males, whereas these metabolites were significantly altered at both 2 and 6 h in females (Supplementary Figure 5 and Figure 3). Significant changes in metabolic profiles of male and female mice were mostly returned to baseline at 24 h postinjection in both tissues when comparing treatments. It is well-established that susceptibility to naphthalene toxicity is greater in female mice than in male mice (Carratt et al., 2019b; Van Winkle et al., 2002). These observations may be attributed to the persistence of metabolic changes related to DNA damage, oxidative stress, and lung remodeling in females but not in males. Furthermore, metabolite changes in males may also indicate protective mechanisms that mitigate naphthalene toxicity compared with females, although this was not a primary focus of our analysis.

The acute toxic effects of naphthalene exposure are well characterized in mice. However, few studies have utilized metabolomics to evaluate the contribution of global lung metabolite changes underlying the mechanism of naphthalene toxicity (Hong et al., 2014; Lee et al., 2018; Ling et al., 2014). Lung metabolomics studies in mice routinely analyze homogenized whole lung lobes, which prevents the characterization of region-specific responses following exposure to toxicants that target individual regions of the lung. The objective of our study was to identify region-specific differences in metabolite profiles from microdissected lung airways and parenchyma of naphthalene-treated mice. The findings from this study identified inherent differences between the metabolite profiles of lung airways and parenchyma, which were further altered by naphthalene treatment. We also found significant differences in multiple metabolite classes related to oxidative stress, DNA damage, and membrane remodeling in both airways and parenchyma treated with naphthalene. Importantly, the responses between male and female mice varied greatly with respect to the duration and extent of significant changes in metabolite profiles, further validating the findings of previous studies. Future experiments are needed to assess the impact of the pharmacokinetic differences

between injected and inhaled naphthalene on the exposure-induced metabolomic changes in different lung regions and to examine the effects of chronic naphthalene exposure to determine whether the acute metabolite changes observed here will persist and ultimately influence the development of lung diseases (Kovalchuk *et al.*, 2020). Nonetheless, the characterization of differences in lung metabolite profiles between lung airways and parenchyma in our study underscores the importance of region-specific metabolomic analysis of lung responses to target-specific toxicants.

SUPPLEMENTARY DATA

Supplementary data are available at *Toxicological Sciences* online.

AUTHOR CONTRIBUTIONS

N.C.S., L.S.V.W, and O.F. prepared the manuscript; N.C.S., L.S.V.W., X.D., and P.C.E. developed the experimental design for the study; N.C.S., L.M.T, and P.C.E. performed the animal experiments and tissue collection; N.C.S. analyzed the data; and all authors contributed to editing the manuscript.

DECLARATION OF CONFLICTING INTERESTS

The authors declared no potential conflicts of interest with respect to the research, authorship, and/or publication of this article.

References

Altmeyer, M., Messner, S., Hassa, P. O., Fey, M., and Hottiger, M. O. (2009). Molecular mechanism of poly(adp-ribosyl)ation by parp1 and identification of lysine residues as adp-ribose acceptor sites. *Nucleic Acids Res.* **37**, 3723–3738.

Barupal, D. K., and Fiehn, O. (2017). Chemical similarity enrichment analysis (chemrich) as alternative to biochemical pathway mapping for metabolomic datasets. *Sci. Rep.* **7**, 14567.

Bonini, P., Kind, T., Tsugawa, H., Barupal, D. K., and Fiehn, O. (2020). Retip: Retention time prediction for compound annotation in untargeted metabolomics. *Anal. Chem.* **92**, 7515–7522.

Bradley, H., Nccoxnell, S. D., and Crystal, R. G. (1974). Lung collagen composition and synthesis. *J. Biol. Chem.* **219**, 2674–2683.

Brunetti, M., Gaiti, A., and Porcellati, G. (1979). Synthesis of phosphatidylcholine and phosphatidylethanolamine at different ages in the rat brain in vitro. *Lipids* **14**, 925–931.

Buckpitt, A., Boland, B., Isbell, M., Morin, D., Shultz, M., Baldwin, R., Chan, K., Karlsson, A., Lin, C., Taff, A., *et al.* (2002). Naphthalene-induced respiratory tract toxicity: Metabolic mechanisms of toxicity. *Drug Metab. Rev.* **34**, 791–820.

Buckpitt, A., Chang, A. M., Weir, A., Van Winkle, L., Duan, X., Philpot, R., and Plopper, C. (1995). Relationship of cytochrome p450 activity to clara cell cytotoxicity. Iv. Metabolism of naphthalene and naphthalene oxide in microdissected airways from mice, rats, and hamsters. *Mol. Pharmacol.* **47**, 74–81.

Buckpitt, A., Morin, D., Murphy, S., Edwards, P., and Van Winkle, L. (2013). Kinetics of naphthalene metabolism in target and non-target tissues of rodents and in nasal and airway microsomes from the rhesus monkey. *Toxicol. Appl. Pharmacol.* **270**, 97–105.

Bundy, J. G., Davey, M. P., and Viant, M. R. (2009). Environmental metabolomics: A critical review and future perspectives. *Metabolomics* **5**, 3–21.

Cajka, T., and Fiehn, O. (2016). Increasing lipidomic coverage by selecting optimal mobile-phase modifiers in LC-MS of blood plasma. *Metabolomics* **12**, 1–11.

Carratt, S. A., Hartog, M., Buchholz, B. A., Kuhn, E. A., Collette, N. M., Ding, X., and Van Winkle, L. S. (2019a). Naphthalene genotoxicity: DNA adducts in primate and mouse airway explants. *Toxicol. Lett.* **305**, 103–109.

Carratt, S. A., Kovalchuk, N., Ding, X., and Van Winkle, L. S. (2019b). Metabolism and lung toxicity of inhaled naphthalene: Effects of postnatal age and sex. *Toxicol. Sci.* **170**, 536–548.

Fan, S., Kind, T., Cajka, T., Hazen, S. L., Tang, W. H. W., Kaddurah-Daouk, R., Irvin, M. R., Arnett, D. K., Barupal, D. K., and Fiehn, O. (2019). Systematic error removal using random forest for normalizing large-scale untargeted lipidomics data. *Anal. Chem.* **91**, 3590–3596.

Gu, Z., Eils, R., and Schlesner, M. (2016). Complex heatmaps reveal patterns and correlations in multidimensional genomic data. *Bioinformatics* **32**, 2847–2849.

Gupta, R., Radicioni, G., Abdelwahab, S., Dang, H., Carpenter, J., Chua, M., Mieczkowski, P. A., Sheridan, J. T., Randell, S. H., and Kesimer, M. (2019). Intercellular communication between airway epithelial cells is mediated by exosome-like vesicles. *Am. J. Respir Cell Mol. Biol.* **60**, 209–220.

Hong, J. H., Lee, W. C., Hsu, Y. M., Liang, H. J., Wan, C. H., Chien, C. L., and Lin, C. Y. (2014). Characterization of the biochemical effects of naphthalene on the mouse respiratory system using NMR-based metabolomics. *J. Appl. Toxicol.* **34**, 1379–1388.

Hou, W. H., Chen, S. H., and Yu, X. (2019). Poly-ADP ribosylation in DNA damage response and cancer therapy. *Mutation Res.* **780**, 82–91.

Jia, C., and Batterman, S. (2010). A critical review of naphthalene sources and exposures relevant to indoor and outdoor air. *Int. J. Environ. Res. Public Health* **7**, 2903–2939.

Jie Yan, Y., Li, Y., Lou, B., and ping Wu, M. (2006). Beneficial effects of APOA-I on LPS-induced acute lung injury and endotoxemia in mice. *Life Sci.* **79**, 210–215.

Kim, T. H., Lee, Y. H., Kim, K. H., Lee, S. H., Cha, J. Y., Shin, E. K., Jung, S., Jang, A. S., Park, S. W., Uh, S. T., *et al.* (2010). Role of lung apolipoprotein A-I in idiopathic pulmonary fibrosis antiinflammatory and antifibrotic effect on experimental lung injury and fibrosis. *Am. J. Respir. Crit. Care Med.* **182**, 633–642.

Koelmel, J. P., Kroeger, N. M., Gill, E. L., Ulmer, C. Z., Bowden, J. A., Patterson, R. E., Yost, R. A., and Garrett, T. J. (2017). Expanding lipidome coverage using LC-MS/MS data-dependent acquisition

with automated exclusion list generation. *J. Am. Soc. Mass Spectrom.* **28**, 908–917.

Kovalchuk, N., Kelty, J., Li, L., Hartog, M., Zhang, Q. Y., Edwards, P., Van Winkle, L., and Ding, X. (2017). Impact of hepatic p450-mediated biotransformation on the disposition and respiratory tract toxicity of inhaled naphthalene. *Toxicol. Appl. Pharmacol.* **329**, 1–8.

Kovalchuk, N., Zhang, Q. Y., Van Winkle, L., and Ding, X. (2020). Contribution of pulmonary cyp-mediated bioactivation of naphthalene to airway epithelial injury in the lung. *Toxicol. Sci.* **177**, 334–346.

Lankadurai, B. P., Nagato, E. G., and Simpson, M. J. (2013). Environmental metabolomics: An emerging approach to study organism responses to environmental stressors. *Environ. Rev.* **21**, 180–205.

Lanza, D. L., Code, E., Crespi, C. L., Gonzalez, F. J., and Yost, G. S. (1999). Specific dehydrogenation of 3-methylindole and epoxidation of naphthalene by recombinant human cyp2f1 expressed in lymphoblastoid cells. *Drug Metab. Dispos.* **27**, 798–803.

Lass, A., Zimmermann, R., Oberer, M., and Zechner, R. (2011). Lipolysis - A highly regulated multi-enzyme complex mediates the catabolism of cellular fat stores. *Progr. Lipid Res.* **50**, 14–27.

Law, S. H., Chan, M. L., Marathe, G. K., Parveen, F., Chen, C. H., and Ke, L. Y. (2019). An updated review of lysophosphatidylcholine metabolism in human diseases. *Int. J. Mol. Sci.* **20**, 1149.

Lee, S. H., Hong, S. H., Tang, C. H., Ling, Y. S., Chen, K. H., Liang, H. J., and Lin, C. Y. (2018). Mass spectrometry-based lipidomics to explore the biochemical effects of naphthalene toxicity or tolerance in a mouse model. *PLoS One* **13**, e0204829.

Li, L., Carratt, S., Hartog, M., Kovalchik, N., Jia, K., Wang, Y., Zhang, Q.-Y., Edwards, P., Winkle, L. V., and Ding, X. (2017). Human cyp2a13 and cyp2f1 mediate naphthalene toxicity in the lung and nasal mucosa of cyp2a13/2f1-humanized mice. *Environ. Health Perspect.* **125**, 067004.

Li, L., Wei, Y., Van Winkle, L., Zhang, Q. Y., Zhou, X., Hu, J., Xie, F., Kluetzman, K., and Ding, X. (2011). Generation and characterization of a cyp2f2-null mouse and studies on the role of cyp2f2 in naphthalene-induced toxicity in the lung and nasal olfactory mucosa. *J. Pharmacol. Exp. Ther.* **339**, 62–71.

Li, Z., Mulholland, J. A., Romanoff, L. C., Pittman, E. N., Trinidad, D. A., Lewin, M. D., and Sjödin, A. (2010). Assessment of non-occupational exposure to polycyclic aromatic hydrocarbons through personal air sampling and urinary biomonitoring. *J. Environ. Monit.* **12**, 1110–1118.

Lin, C. Y., Huang, F. P., Ling, Y. S., Liang, H. J., Lee, S. H., Hu, M. Y., and Tsao, P. N. (2015). Use of nuclear magnetic resonance-based metabolomics to characterize the biochemical effects of naphthalene on various organs of tolerant mice. *PLoS One* **10**, e0120429.

Ling, Y. S., Liang, H. J., Chung, M. H., Lin, M. H., and Lin, C. Y. (2014). NMR- and MS-based metabolomics: Various organ responses following naphthalene intervention. *Mol. BioSyst.* **10**, 1918–1931.

Ninou, I., Magkrioti, C., and Aidinis, V. (2018). Autotaxin in pathophysiology and pulmonary fibrosis. *Front. Med.* **5**, 180.

NTP. (2000). NTP technical report on the toxicology and carcinogenesis studies of naphthalene in f344 n rats (inhalation studies). National Toxicology Program, Research Triangle Park, NC.

Oikonomou, N., Mouratis, M.-A., Tzouvelekis, A., Kaffe, E., Valavanis, C., Vilaras, G., Karameris, A., Prestwich, G. D.,

Bouros, D., and Aidinis, V. (2012). Pulmonary autotaxin expression contributes to the pathogenesis of pulmonary fibrosis. *Am. J. Respir. Cell Mol. Biol.* **47**, 566–574.

Phimister, A. J., Lee, M. G., Morin, D., Buckpitt, A. R., and Plopper, C. G. (2004). Glutathione depletion is a major determinant of inhaled naphthalene respiratory toxicity and naphthalene metabolism in mice. *Toxicol. Sci.* **82**, 268–278.

Plopper, C. G., Chang, A. M., Pang, A., and Buckpit, A. R. (1991). Use of microdissected airways to define metabolism and cytotoxicity in murine bronchiolar epithelium. *Experim. Lung Res.* **17**, 197–212.

Plopper, C. G., Suverkropp, C., Morin, D., Nishio, S., and Buckpitt, A. (1992). Relationship of cytochrome p-450 activity to clara cell cytotoxicity. I. Histopathologic comparison of the respiratory tract of mice, rats and hamsters after parenteral administration of naphthalene. *J. Pharmacol Exp. Ther.* **261**, 353–363.

Plopper, C. G., Van Winkle, L. S., Fanucchi, M. V., Malburg, S. R., Nishio, S. J., Chang, A., and Buckpitt, A. R. (2001). Early events in naphthalene-induced acute clara cell toxicity ii. Comparison of glutathione depletion and histopathology by airway location. *Am. J. Respir. Cell Mol. Biol.* **24**, 272–281.

Rice, S. J., Liu, X., Miller, B., Joshi, M., Zhu, J., Caruso, C., Gilbert, C., Toth, J., Reed, M., Rassaei, N., *et al.* (2015). Proteomic profiling of human plasma identifies apolipoprotein E as being associated with smoking and a marker for squamous metaplasia of the lung. *Proteomics* **15**, 3267–3277.

Ruiz-Perez, D., Guan, H., Madhivanan, P., Mathee, K., and Narasimhan, G. (2020). So you think you can pls-da? *BMC Bioinformatics* **21**, 2.

Satoh, M. S., and Lindahl, T. (1992). Role of poly(ADP-ribose) formation in DNA repair. *Nature* **356**, 356–358.

Shultz, M. A., Choudary, P. V., and Buckpitt, A. R. (1999). Role of murine cytochrome p-450 2f2 in metabolic activation of naphthalene and metabolism of other xenobiotics 1. *J. Pharmacol. Exp. Ther.* **290**, 281–288.

Tsugawa, H., Cajka, T., Kind, T., Ma, Y., Higgins, B., Ikeda, K., Kanazawa, M., Vandergheynst, J., Fiehn, O., and Arita, M. (2015). MS-dial: Data-independent MS/MS deconvolution for comprehensive metabolome analysis. *Nat. Methods* **12**, 523–526.

Van Winkle, L. S., Gunderson, A. D., Shimizu, J. A., Baker, G. L., and Brown, C. D. (2002). Gender differences in naphthalene metabolism and naphthalene-induced acute lung injury. *Am. J. Physiol. Lung Cell. Mol. Physiol.* **282**, L1122–L1134.

Wang, B., and Tontonoz, P. (2019). Phospholipid remodeling in physiology and disease. *Annu. Rev. Physiol.* **81**, 165–188.

Worley, B., and Powers, R. (2012). Multivariate analysis in metabolomics. *Curr. Metab.* **1**, 92–107.

Yao, X., Gordon, E. M., Figueroa, D. M., Barochia, A. V., and Levine, S. J. (2016). Emerging roles of apolipoprotein E and apolipoprotein A-I in the pathogenesis and treatment of lung disease. *Am. J. Respir. Cell Mol. Biol.* **55**, 159–169.

Yoder, M., Zhuge, Y., Yuan, Y., Holian, O., Kuo, S., van Breemen, R., Thomas, L. L., and Lum, H. (2014). Bioactive lysophosphatidylcholine 16:0 and 18:0 are elevated in lungs of asthmatic subjects. *Allergy Asthma Immunol. Res.* **6**, 61–65.

Zhang, Y., Yu, W., Han, D., Meng, J., Wang, H., and Cao, G. (2019). L–lysine ameliorates sepsis-induced acute lung injury in a lipopolysaccharide-induced mouse model. *Biomed. Pharmacother.* **118**, 109307.